Clays and Clay Minerals, Vol. 40, No. 5, 491–500, 1992.

THE EFFECT OF UNEQUAL IONIC SIZE ON THE SWELLING PRESSURE IN CLAYS

MARLENE M. HUERTA, JOAN E. CURRY, AND DONALD A. MCQUARRIE

Department of Chemistry and the Institute of Theoretical Dynamics
University of California, Davis, California 95616-5295

Abstract—In this paper, we use the unequal radius modified Gouy-Chapman theory to evaluate the effect of the ionic size of the electrolyte on the swelling pressures (Π) in different clay systems immersed in electrolytic solutions. First the model is applied to a 1:1 electrolyte to show that the coion size is only important at surface charge densities much lower than those found in typical clay systems. The swelling pressure is calculated and the results are compared with experimental data. Literature ionic radii values are used to show the dependence of the swelling pressure on the specific counterions present. Next the model is applied to a 1:1 and 2:1 electrolyte mixture with unequal-sized counterions to show the swelling pressure is highly dependent on both counterion sizes. The unequal and same-sized cases are compared.

Key Words—Clay, Swelling pressure, Unequal ion size.

INTRODUCTION

Clay swelling is important in many applications including petroleum engineering, soil permeability, waste disposal liner design and the development of many commercially available consumer products. Swelling is thought to be caused primarily by hydration of the clay surfaces at small separations and electrical double layer overlap at large separations. Most of the electrolyte ions in the electrical double layer are found in a narrow region near the charged surface. Finite ion size effects are expected to be most significant in this region. Finite size is usually accounted for by modifying the Poisson-Boltzmann formalism to allow for a region the width of a hydrated ion near the surface in which no charge is found. Given that ionic species are of different size, we will investigate the effect of the unequal size of the electrolyte within the Poisson-Boltzmann theory in the study of clay swelling.

Some effort to understand the effect of unequal ionic sizes of the electrolyte on the electrostatic properties of the electrical double layer has been made in the last ten years. A non-zero potential at the electrode in the absence of a surface charge (potential-of-zero-charge) was found for a one-wall system by Valleau and Torrie (1982). That phenomenon was usually attributed to specific adsorption at the electrode, but it seems that it can be accounted for, at least in part, by introducing unequal ionic diameters. Bhuiyan *et al.* (1983) also reported the effect of considering different sizes in the electrolyte in a one-wall system using the nonlinear Poisson-Boltzmann equation and found results in agreement with Valleau and Torrie (1982).

However the corresponding problem of the interaction between two planar surfaces has just recently received attention. McBroom and McQuarrie (1987) reported the effect of the unequal size of the electrolyte on the electrostatic force between two planar surfaces in a 1:1 electrolyte using the nonlinear Poisson-Boltzmann equation. The prediction of a non-zero force between two uncharged walls was an interesting result.

We will use the unequal-radius-modified-Gouy-Chapman (URMGC) approach to the interaction of two charged surfaces, introduced by McBroom and McQuarrie (1987), to describe the electrostatic interaction of two clay surfaces that are immersed in an electrolytic solution. First we consider a 1:1 electrolyte with an unequal-sized cation and anion. We will show that the anion size is not important in clay swelling. Secondly, due to the importance of clay stability problems, we apply the unequal radius model to a 1:1 and 2:1 electrolyte mixture such as NaCl and $CaCl_2$ to show the dependence of the swelling pressure on both counterion sizes.

THEORY

Unequal radius model for a 1:1 electrolyte

We model the clay surfaces as a two-wall system with a uniform surface charge density σ_0 ($\sigma_0 < 0$) immersed in an aqueous electrolyte solution. The solution is modelled by the unrestricted primitive model, where the ions are considered as hard spheres with the cation of radius R_+ with a charge z_+e and the anion of radius R_- with a charge z_-e, where e ($e > 0$) is the protonic charge. In the first case we will consider a symmetrical, univalent salt with $z_+ = -z_- = 1$.

The Poisson-Boltzmann equation for this system is

$$\frac{d^2\phi}{d\xi^2} = -\sum_i \frac{z_i}{2}\exp(-z_i\phi) \qquad (1)$$

where $\xi = \kappa x$, with ξ the distance from one of the walls and $\kappa^2 = 2e^2c_0/\epsilon_0\epsilon kT$ the usual Debye-Hückel parameter, c_0 is the bulk number density of electrolyte, $\phi = e\psi/kT$ is a reduced electrostatic potential, ϵ is the dielectric constant, k is the Boltzmann constant, and T

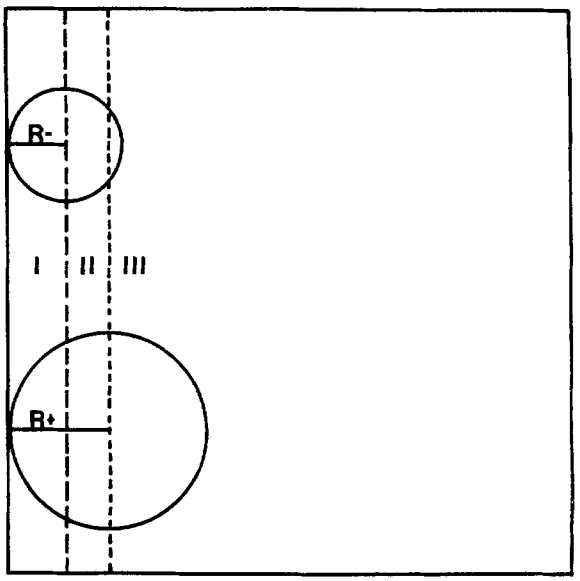

Figure 1. The model and geometry used in the 1:1 electrolyte system. The large cation case is shown.

is the Kelvin temperature. For the case of unequal-sized ions, Eq. (1) must be solved separately in three different regions. We choose x as the distance from the wall to the point of interest, as shown in Figure 1. The two cases where either the cation or anion is the larger ion must be considered separately. We shall treat the case in which the cation is larger first.

In region I of Figure 1, no charges are present between the wall x = 0 and the radius of the (smaller) anion, R_-, and so Eq. (1) reads

$$\frac{d^2\phi}{d\xi^2} = 0 \qquad 0 < \xi < \xi_- = \kappa R_-. \tag{2}$$

In region II, only negative charges are present, and so we have

$$\frac{d^2\phi}{d\xi^2} = \frac{e^{\phi}}{2} \qquad \xi_- < \xi < \xi_+ = \kappa R_+. \tag{3}$$

In region III, both positive and negative charges are allowed, and so we have

$$\frac{d^2\phi}{d\xi^2} = \sinh \phi \qquad \xi_+ < \xi < \xi_d = \kappa d \tag{4}$$

where 2d is the distance between the plates. It is only necessary to work from x = 0 to x = d because of the symmetry of the system.

The boundary conditions are given by:

a) $$\frac{d\phi^{I}}{d\xi} = -\frac{e\sigma_0}{\epsilon_0 \epsilon \kappa kT} \equiv -\sigma_0^* \qquad \xi = 0 \tag{5}$$

b) $$\epsilon \frac{d\phi^{I}}{d\xi} = \epsilon \frac{d\phi^{II}}{d\xi} \qquad \xi = \xi_- \tag{6}$$

where I and II represent region I and region II, respectively;

c) $$\epsilon \frac{d\phi^{II}}{d\xi} = \epsilon \frac{d\phi^{III}}{d\xi} \qquad \xi = \xi_+ \tag{7}$$

where II and III represent region II and region III, respectively;

d) $$\frac{d\phi}{d\xi} = 0 \qquad \xi = \xi_d. \tag{8}$$

The continuity of electrostatic potential at $x = R_-$ and at $x = R_+$ is also used. The dielectric constant ϵ is considered to be the same for all three regions.

In the case in which the anion is the larger ion, Eqs. (2), (3), and (4) are

$$\frac{d^2\phi}{d\xi^2} = 0 \qquad 0 < \xi < \xi_+ \tag{9}$$

$$\frac{d^2\phi}{d\xi^2} = -\frac{e^{-\phi}}{2} \qquad \xi_+ < \xi < \xi_- \tag{10}$$

$$\frac{d^2\phi}{d\xi^2} = \sinh \phi \qquad \xi_- < \xi < \xi_d \tag{11}$$

with R_+ and R_- interchanged in Eqs. (5) through (8).

We shall use the **large cation case** to illustrate the solution to the above equations. Using boundary conditions (5) the solution of Eq. (2) is

$$\phi(\xi) = \phi(0) - \sigma_0^* \xi \qquad 0 < \xi < \xi_-. \tag{12}$$

The first integration of Eq. (3) gives

$$\frac{d\phi}{d\xi} = [e^{\phi} + A]^{1/2} \qquad \xi_- < x < \xi_+ \tag{13}$$

where A is a constant of integration. We must explicitly consider two possibilities for the sign of A. For the two cases $A < 0$ and $A > 0$ respectively, we write Eq. (13) as

$$\frac{d\phi}{d\xi} = [e^{\phi} - \beta^2]^{1/2} \qquad A < 0 \tag{14}$$

and

$$\frac{d\phi}{d\xi} = [e^{\phi} + \alpha^2]^{1/2} \qquad A > 0 \tag{15}$$

where α and β are real constants. These two equations can be integrated once more to give, Gradshteyn and Ryzhik (1980),

$$(\xi - \gamma) = \frac{2}{\beta} \tan^{-1}\left(\frac{(e^{\phi} - \beta^2)^{1/2}}{\beta}\right) \qquad A < 0 \tag{16}$$

and

$$(\xi - \gamma) = \frac{1}{\alpha} \ln\left\{\frac{(e^{\phi} + \alpha^2)^{1/2} - \alpha}{(e^{\phi} + \alpha^2)^{1/2} + \alpha}\right\} \qquad A > 0 \tag{17}$$

where γ is another integration constant.

Eqs. (16) and (17) should transform into one another

https://doi.org/10.1346/CCMN.1992.0400502 Published online by Cambridge University Press

under the transformation $\alpha = i\beta$ or $\beta = i\alpha$. To see that this is so, we let $\alpha = i\beta$ in Eq. (17) and use the identity $\tan^{-1}z = (i2)\ln\{(1 - iz)/(1 + iz)\}$ with $z = \beta/(e^{\phi} - \beta^2)^{1/2}$ to obtain:

$$\frac{1}{\alpha}\ln\left\{\frac{(e^{\phi} + \alpha^2)^{1/2} - \alpha}{(e^{\phi} + \alpha^2)^{1/2} + \alpha}\right\} = -\frac{2}{\beta}\tan^{-1}\left\{\frac{\beta}{(e^{\phi} - \beta^2)^{1/2}}\right\}. \quad (18)$$

By using the identity

$$\tan^{-1}(1/z) = \pi/2 - \tan^{-1}z \quad (19)$$

Eqs. (17) and (18) become

$$(\xi - \gamma) = \frac{2}{\beta}\left\{\tan^{-1}\left[\frac{(e^{\phi} - \beta^2)^{1/2}}{\beta}\right] - \frac{\pi}{2}\right\} \quad (20)$$

which is equivalent to Eq. (16). Furthermore, by using the two expansions $\ln\{(1 - z)/(1 + z)\} = -2z + O(z^3)$ and $\tan^{-1}z = \pi/2 - 1/z + 1/3z^3 + \ldots$, we see that both Eqs. (17) and (20) reduce to

$$\xi - \gamma = -2e^{-\phi/2} \quad (21)$$

in the limits $\alpha \to 0$ and $\beta \to 0$.

By starting with

$$(\xi - \gamma) = -\frac{2}{\beta}\tan^{-1}\left\{\frac{\beta}{(e^{\phi} - \beta^2)^{1/2}}\right\} \quad (22)$$

and subtracting it at ξ_- from it at ξ_+, and then using Eq. (6), we obtain

$$\xi_+ - \xi_- = -\frac{2}{\beta}\left[\tan^{-1}\left\{\frac{\beta}{(e^{\phi_+} - \beta^2)^{1/2}}\right\} - \tan^{-1}\left\{\frac{\beta}{-\sigma_0^*}\right\}\right] \quad (23)$$

where ϕ_+ represents $\phi(\kappa R_+) = e\psi(R_+)/kT$.

The integration constant γ is obtained by evaluating Eq. (22) at $\xi = \xi_+$ and subtracting it from Eq. (33) to get

$$\gamma = \xi_- + \frac{2}{\beta}\tan^{-1}\left\{\frac{\beta}{-\sigma_0^*}\right\}. \quad (24)$$

We can use Eq. (23) to write

$$e^{\phi_+} = \frac{\beta^2}{\sin^2\chi} \qquad A < 0 \quad (25)$$

where

$$\chi = -\frac{\beta}{2}(\xi_+ - \xi_-) + \tan^{-1}\left\{\frac{\beta}{-\sigma_0^*}\right\}. \quad (26)$$

Solving Eq. (22) for $\varphi(\xi)$, we write the electrostatic potential in Region II for $A < 0$ as

$$\phi(\xi) = \ln\left[\frac{\beta^2}{\sin^2\theta}\right] \qquad \xi_- < \xi < \xi_+ \quad (27)$$

where

$$\theta = -\frac{\beta}{2}(\xi - \gamma). \quad (28)$$

The potential at $x = R_-$ is obtained by using the boundary conditions (5) and (6) and Eq. (14)

$$\varphi_- = \ln[(-\sigma_0^*)^2 + \beta^2]. \quad (29)$$

Similarly, starting with Eq. (17) for the $A > 0$ case, we can write

$$\gamma = -\xi_- - \frac{2}{\alpha}\ln\left\{\frac{\alpha + -\sigma_0^*}{(-\sigma_0^*)^2 - \alpha^2}\right\} \quad (30)$$

and

$$e^{\phi_+} = \frac{\alpha^2}{\sinh^2\eta} \qquad A > 0 \quad (31)$$

where

$$\eta = -\frac{\alpha}{2}(\xi_+ - \xi_-) + \ln\left\{\frac{\alpha - \sigma_0^*}{[(-\sigma_0^*)^2 - \alpha^2]^{1/2}}\right\}. \quad (32)$$

Solving Eq. (17) for $\phi(\xi)$, we write the electrostatic potential in Region II for $A > 0$ as

$$\phi(\xi) = \ln\left[\frac{\alpha^2}{\sinh^2 T}\right] \qquad \xi_- < \xi < \xi_+ \quad (33)$$

with

$$T = -\frac{\alpha}{2}(\xi + \gamma). \quad (34)$$

Now the electrostatic potential at $\xi = \xi_-$ is given by

$$\varphi_- = \ln((-\sigma_0^*)^2 - \alpha^2). \quad (35)$$

Eqs. (25) and (31) are converted one into the other by considering β real ($A < 0$) or pure imaginary, $i\alpha$ ($A > 0$).

Eq. (6) can be solved using boundary conditions (5–8), so that

$$\frac{d\phi}{d\xi} = 2^{1/2}[\cosh\phi - \cosh\phi_d]^{1/2} \quad (36)$$

where ϕ_d is the (reduced) electrostatic potential at the midpoint, d. Letting $y = \cosh\phi$, Eq. (36) can be integrated to give

$$\int_0^{(y_+ - y_d)} \frac{dy}{[y((y + y_d)^2 - 1)]^{1/2}} = 2^{1/2}\kappa(d - R_+) \quad (37)$$

where

$$y_d = \cosh\phi_d \qquad \text{and} \qquad y_+ = \cosh\phi_+.$$

Using the boundary condition given by Eq. (7) to equate Eqs. (36) and (14), we eventually obtain y_d and $(y_+ - y_d)$, the integration limit in Eq. (37) in terms of β:

$$y_d = \frac{1}{2}\left(\frac{\sin^2\chi}{\beta^2} + \beta^2\right) \quad (38)$$

https://doi.org/10.1346/CCMN.1992.0400502 Published online by Cambridge University Press

with $\chi(\beta)$ given by Eq. (26) and

$$(y_+ - y_d) = \frac{\beta^2}{2}\left(\frac{1}{\sin^2\chi} - 1\right). \quad (39)$$

Likewise, using Eq. (7) to equate Eqs. (36) and (15), we can also write y_d and $(y_+ - y_d)$ in terms of α:

$$y_d = \frac{1}{2}\left(\frac{\sin^2\eta}{\alpha^2} + \alpha^2\right) \quad (40)$$

$$y_+ - y_d = \frac{\alpha^2}{2}\left(\frac{1}{\sinh^2\eta} + 1\right). \quad (41)$$

The only independent variable in Eq. (37) is either α or β, through y_+ and y_d. To avoid the singularity at $y = 0$, we add and subtract the factor

$$\frac{1}{y^{1/2}(y_d^2 - 1)^{1/2}} \quad (42)$$

in the integrand. Eq. (37) is then rewritten

$$\int_0^{(y_+ - y_d)} \frac{dy[y_d^2 - 1]^{1/2} - [(y + y_d)^2 - 1]^{1/2}}{[y\cdot[(y + y_d)^2 - 1][y_d^2 - 1]]^{1/2}} + 2\left[\frac{y_+ - y_d}{y_d^2 - 1}\right] = 2^{1/2}\kappa(d - R_+). \quad (43)$$

In order to solve Eq. (43) iteratively, the value of the integration constant α or β is varied until the left-hand side and right-hand side of the equation are equal each to the other. The problem can be solved by writing y_d and $y_+ - y_d$ in terms of either α or β. For instance, in using the solution as written in Eqs. (38) through (39), β is real for $A < 0$ and imaginary for $A > 0$. On the other hand, if the solution is written in terms of α as in Eqs. (40) and (41), α will be real for $A > 0$ and imaginary for $A < 0$. The integral on the left-hand side of Eq. (43) was evaluated using the Composite Simpson rule algorithm. Once the value of α or β is obtained the values of $\phi(\xi)$ in Region III are found by solving

$$\int_0^{(y - y_d)} \frac{dy'[[y_d^2 - 1]^{1/2} - [(y' + y_d)^2 - 1]^{1/2}]}{[y'[(y' + y_d)^2 - 1][y_d^2 - 1]]^{1/2}} + 2\left[\frac{y - y_d}{y_d^2 - 1}\right]^{1/2} = 2^{1/2}(\xi_d - \xi) \quad (44)$$

for each value of ξ between $\xi = \kappa R_-$ and $\xi = \kappa d$. This is done by varying y until both sides of Eq. (44) are the same for each ξ.

We found that A is less than zero for small values of charge density and A is greater than zero for large values of charge density. The equations with $A > 0$ involve a numerical subtlety. To appreciate this subtlety, consider Eq. (35), which we can write as

$$e^{\phi_-} = (-\sigma_0^*)^2 - \alpha^2 \quad (45)$$

where α is to be determined numerically. For typical values of the clay minerals that we are considering, ϕ_- is of the order -10 and $-\sigma_0^*$ is of the order 200. Consequently, Eq. (30) demands that the difference between α and σ_0^* must be of the order 10^{-7}. In order to find a good initial guess for α, Eq. (32) is rewritten as

$$\eta = -\frac{\alpha}{2}(\xi_+ - \xi_-) + \frac{1}{2}\ln\left\{\frac{(-\sigma_0)^* + \alpha}{(-\sigma_0)^* - \alpha}\right\}. \quad (46)$$

But because $(\sigma_0^* - \alpha)$ is $O(10^{-7})$, we write this equation as

$$\eta = -\frac{-\sigma_0^*}{2}(\xi_+ - \xi_-) + \frac{1}{2}\ln\left\{\frac{(-2\sigma_0^*)}{(-\sigma_0^* - \alpha)}\right\}. \quad (47)$$

Eq. (47) is solved for α and this value is used as an initial guess in the unmodified Eqs. (40) and (41). The iteration is carried out until Eq. (43) is satisfied.

In the **large anion case**, only the equations involving $A < 0$ needed to be solved in order to calculate electrostatic potential profiles for all distances between the walls, surface charge densities, and concentrations. The key equations for this case are:

$$\gamma - \xi = -\frac{2}{\beta}\tan^{-1}\left\{\frac{\beta}{(e^{-\phi} - \beta^2)^{1/2}}\right\} \quad (48)$$

and

$$e^{-\phi_-} = \frac{\beta^2}{\sin^2\chi} \quad (49)$$

with χ still given by Eq. (26).

The electrostatic potential profile in Region I is given by Eq. (12) with ξ_- replaced by ξ_+. The equations for electrostatic potential profile in Region II can be derived by using Eq. (48) and solving for $\phi(\xi)$

$$\phi(\xi) = -\ln\left[\frac{\beta^2}{\sin^2\delta}\right] \qquad \xi_+ < \xi < \xi_- \quad (50)$$

where

$$\delta = -\frac{\beta}{2}(\gamma - \xi). \quad (51)$$

We can evaluate γ by equating $e^{-\phi_-}$ from Eq. (49) and Eqs. (50) and (51) evaluated at $\xi_- = \kappa R_-$:

$$\gamma = \xi_+ - \frac{2}{\beta}\tan^{-1}\left\{\frac{\beta}{-\sigma_0^*}\right\}. \quad (52)$$

The values for $\phi(\xi)$ in Region III are obtained by solving Eq. (44) as in the large cation case.

The pressure between the surfaces due to the electrical double layer interaction is given by

$$P = 2c_0kT(\cosh\phi_d - 1) \quad (53)$$

where $\phi_d = \psi_d e/kT$; ψ_d is the electrostatic potential midway between the surfaces. The total interaction between the surfaces is the sum of this electrostatic force and the (attractive) van der Waals force

$$f = \frac{-B}{6\pi h^3} \quad (54)$$

where $h = 2d$ is the separation between the surfaces

https://doi.org/10.1346/CCMN.1992.0400502 Published online by Cambridge University Press

and B is the Hamaker constant, usually taken as 2.2 $\times 10^{-20}$ joules.

Unequal radius model for a 1:1 and 2:1 mixture

In this case we will consider a mixture composed of a small divalent cation, $z_{2+} = 2$, a large monovalent cation, $z_+ = 1$, and a common anion, $z_- = -1$, the same size as the large cation shown in Figure 2. The total electrolyte concentration, n_{total}, is the sum of the divalent, n_{2+}, and the monovalent, n_{1+}, bulk electrolyte concentrations. The parameter $t = n_{2+}/n_{total}$ is the percentage of divalent electrolyte present. The system is otherwise as described for the 1:1 system. The Poisson-Boltzmann is again solved in three regions.

In Region I of Figure 2, no charges are present between the wall $x = 0$ and the radius of the divalent cation, R_{2+}, and so Eq. (1) reads

$$\frac{d^2\phi}{d\xi^2} = 0 \qquad 0 < \xi < \xi_{2+} = \kappa R_{2+}. \tag{55}$$

In Region II, only positive divalent charges are present, and so we have

$$\frac{d^2\phi}{d\xi^2} = -t \exp(-2\phi) \qquad \xi_{2+} < \xi < \xi_+ = \kappa R_{2+}. \tag{56}$$

In Region III, all electrolyte species are allowed and so we have

$$\frac{d^2\phi}{d\xi^2} = t(-\exp(-2\phi) + \exp\phi) + (1 - t)\sinh\phi \qquad \xi_+ < \xi < \xi_d \tag{57}$$

where Eq. (4) for a 1:1 electrolyte is recovered when $t = 0$. The boundary conditions are given by Eq. (5) and (8). Additionally, the electric field $d\phi/d\xi$ and the electrostatic potential are continuous throughout.

The Region I solution is given by Eq. (12). In Region II after the first integration we have

$$\frac{d\phi}{d\xi} = [t \exp(-2\phi) + A]^{1/2}. \tag{58}$$

Once again we must consider the two possibilities for the sign of A:

$$\frac{d\phi}{d\xi} = [t \exp(-2\phi) - \beta^2]^{1/2} \qquad A < 0 \tag{59}$$

$$\frac{d\phi}{d\xi} = [t \exp(-2\phi) + \alpha^2]^{1/2} \qquad A > 0. \tag{60}$$

Following the derivation of Eqs. (25), (26), (31), and (32), we derive corresponding expressions for the mixture case

$$t \exp(-2\phi) = \frac{\beta^2}{\sin^2\chi} \qquad A < 0 \tag{61}$$

$$\chi = \beta(\xi_1 - \xi_2) + \tan^{-1}\left(\frac{\beta}{-\sigma_0^*}\right) \tag{62}$$

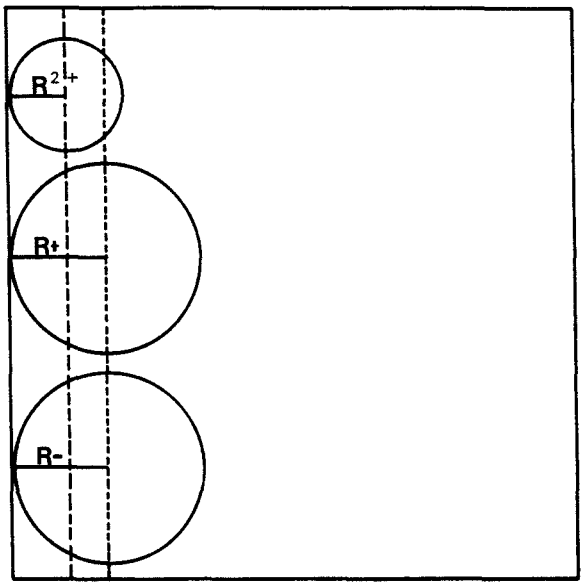

Figure 2. The model and geometry used in the mixed 1:1 and 2:1 electrolyte system.

$$t \exp(-2\phi) = \frac{\alpha^2}{\sinh^2\eta} \qquad A > 0 \tag{63}$$

$$\eta = \alpha(\xi_1 - \xi_2) + \ln\left(1\frac{\alpha - \sigma_0^*}{((-\sigma_0^*)^2 - \alpha^2)^{1/2}}\right). \tag{64}$$

Eq. (57) can be solved using boundary conditions (5)–(8) so that

$$\frac{d\phi}{d\xi} = [t \exp(-2\phi) + 2t \exp\phi + 2(1 - t)\cosh\phi + C] \tag{65}$$

where C is an integration constant. Equating the Region II and III derivatives of the potential at the boundary of the large cation, the integration constant can be written

$$C = \alpha^2 - 2t \sinh\phi_+ - 2\cosh\phi_+ \qquad A > 0 \tag{66}$$

$$C = -\beta^2 - 2t \sinh\phi_+ - 2\cosh\phi_+ \qquad A < 0. \tag{67}$$

Letting $z = \exp\phi$ and $y = z - z_d$, Eq. (65) can be integrated to give

$$-\int_0^{(z_+ - z_d)} \frac{dy}{[y(y - B_1)(y - B_2)(t + 1)]^{1/2}} = \kappa(d - R_+) \tag{68}$$

where

$$B_1 = \frac{a + b}{2(t + 1)}, \qquad B_2 = \frac{a - b}{2(t + 1)},$$
$$a = -[3(t + 1)z_d + C] \tag{69}$$

https://doi.org/10.1346/CCMN.1992.0400502 Published online by Cambridge University Press

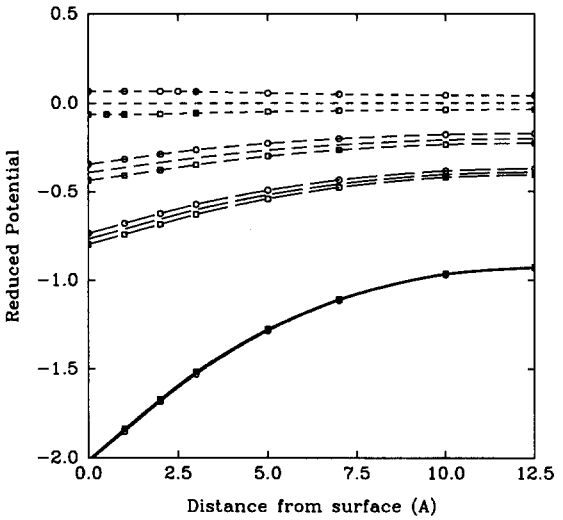

Figure 3. Electrostatic potential profiles in units of kT/e for several surface charge densities between two plates 25Å apart in an electrolyte solution of 0.10 M. The surface charge densities are -0.030 C/m² (solid line), -0.010 C/m² (long dashed line), -0.0050 C/m² (medium dashed line) and 0.00 C/m² (short dashed line). The large cation case ($R_+ = 2.0$, $R_- = 1.0$) is marked with circles, the large anion case ($R_+ = 2.0$, $R_- = 3.0$) is marked with squares and the symmetric case ($R_+ = 2.0$, $R_- = 2.0$) is unmarked.

$$b = [-3(t + 1)^2 z_d^2 - 2C(t + 1)z_d + C^2 - 4(-t^2 + 1)]^{1/2} \quad (70)$$

$$z_+ = \exp \phi_+ \quad \text{and} \quad z_d = \exp \phi_d.$$

Using Eq. (61) and (63), z_+ can be written in terms of α and β:

$$z_+ = \left[\frac{t \sin^2\chi}{\beta^2}\right]^{1/2} \quad (71)$$

and

$$z_+ = \left[\frac{t \sinh^2\eta}{\alpha^2}\right]^{1/2}. \quad (72)$$

With the boundary condition at the midpoint given by Eq. (8), Eq. (65) is rearranged to give a cubic equation for z_d:

$$(t + 1)z_d^3 + Cz_d^2 + (1 - t)z_d + t = 0 \quad (73)$$

where the α or β dependence is in the constant C. There are three possible roots; however, only one root gives a sensible value for z_d. Eq. (68) can be written in terms of either α or β via the expressions for z_+ and z_d. In order to avoid the singularity at y = 0 in the integrand of Eq. (68) we add and subtract

$$-\int_0^{(z_+ - z_d)} \frac{dy}{[y[t + 1]B_1 \cdot B_2]^{1/2}} \quad (74)$$

so that

$$-\int_0^{(z_+ - z_d)} \frac{dy[(y - B_1)(y - B_2)]^{1/2} - (B_1 \cdot B_2)^{1/2}}{[(y - B_1)(y - B_2)y(t + 1)B_1 \cdot B_2]^{1/2}} + 2\left[\frac{z_+ - z_d}{(t + 1)B_1 \cdot B_2}\right]^{1/2} = \kappa(d - R_+). \quad (75)$$

Eq. (75) is solved iteratively in terms of either α or β as described above for the large anion case. The integral was solved using MATHCAD on an IBM AT compatible desktop computer and also using a Gaussian quadrature algorithm on a VAX 750. The numerical difficulties encountered in the large cation case were not found in the mixture case since the anion was never considered to be the closest species to the wall. The electrostatic potential profile can be calculated by using the mixture equations. The electrostatic pressure between the surfaces for a 1:1 and 2:1 mixture is

$$P = kTn_{tot}\left[(t + 1)z_d + \frac{t}{z_d^2} - (t + 2) + \frac{(1 - t)}{z_d}\right] \quad (76)$$

and the swelling pressure is the sum of the electrostatic force and the van der Waals attraction given by Eq. (54).

RESULTS AND DISCUSSION

The importance of the Unequal Radius model for a 1:1 electrolyte depends on the system conditions. For cases of high surface charge density, such as those encountered in clay systems (-0.10 to -0.20 C/m²), the electrostatic profile depends only on the cation size. The calculated profiles using the unsymmetric model considering the anion either larger or smaller than the cation coincide exactly with the profile of a symmetrical system considering the anion to be the same size as the cation.

In order to demonstrate that the coion is only important at surface charge densities much lower than those typical of swelling clays we compare the unequal and same size cases at different charge densities. In Figure 3 we present reduced electrostatic potential profiles for a concentration of 0.10 M, a distance between the walls of 2d = 25Å and at surface charge densities of 0, -0.0050, -0.010 and -0.030 C/m². At each surface charge density we contrast the results obtained from the large anion ($R_+ = 2.0$, $R_- = 3.0$) and large cation ($R_+ = 2.0$, $R_- = 1.0$) cases with those of the symmetrical ($R_+ = 2.0$, $R_- = 2.0$) case. The figure shows deviations from the symmetrical model occur at low surface charge density with the greatest difference being at $\sigma = 0$.

In order to contrast the effect of concentration on the model, the reduced electrostatic potential evaluated at the radius of the cation for the $R_+ > R_-$ case, ϕ_+,

https://doi.org/10.1346/CCMN.1992.0400502 Published online by Cambridge University Press

Table 1. Reduced potential ϕ_+ at R_+ for different values of surface charge density.

Large cation case
Unsymmetrical case corresponds to $R_- = 2.0$ Å and $R_+ = 4.6$ Å.
Symmetrical case corresponds to $R_+ = R_- = 4.6$ Å

c = 0.10 M
d = 14.6 Å

	Symmetrical	Unsymmetrical
σ_o (C/m²)	ϕ_+	ϕ_+
−0.0010	−0.069	−0.208
−0.10	−0.669	−0.739
−0.050	−2.407	−2.407

c = 10^{-4} M
d = 14.6 Å

	Symmetrical	Unsymmetrical
σ_o (C/m²)	ϕ_+	ϕ_+
−0.00005	−1.682	−1.691
−0.00010	−2.350	−2.352
−0.050	−9.284	−9.284

for different surface charge densities at c = 0.10M is presented in Table 1 for both the unsymmetrical case with $R_+ = 4.6$Å and $R_- = 2.0$Å and for the symmetrical case with $R_+ = 4.6$Å and $R_- = 4.6$Å. Note that ϕ_+ in the unsymmetrical case becomes exactly equal to the ϕ_+ in the symmetrical case when the surface charge density becomes higher. In more dilute electrolytic solution, i.e., c = 10^{-4} M, this effect occurs at even lower values of charge density. Thus, for the clay systems in a 1:1 electrolyte, the system of two different size ions behaves as a system of the same size ions, with the size being equal to that of the counterion. As one might expect, the radius of the coion is irrelevant.

It may be desirable for systems other than clays to be able to quantitatively determine when the coion size is important. The following analysis is presented for that purpose. The range in which the unsymmetrical model is useful depends on the surface charge density, electrolyte concentration, ionic radii and the distance between the surfaces. In the limit of the same size counterion and coion, the integration constant, $-\beta^2$ or α^2, in Eqs. (14) and (15) approaches $(-\sigma_0^*)^2$. We may use this to derive an equation which shows the conditions under which the unsymmetrical case is important.

Eq. (45) may be written

$$e^{\phi_-} = (-\sigma_0^* + \alpha)(-\sigma_0^* - \alpha) \cong (-2\sigma_0^*)(-\sigma_0^* - \alpha) \quad (77)$$

where $\alpha \sim -\sigma_0^*$ has been used. Rearranging,

$$\frac{e^{\phi_-}}{-2\sigma_0^*} = (-\sigma_0^* - \alpha) \ll 1. \quad (78)$$

If this condition is satisfied then the system behaves as a symmetrical electrolyte. In a negatively charged system ϕ_- is a negative number so the condition is satisfied when either $|\phi_-|$ or $|\sigma_0^*|$ is large.

In order to determine if $|\phi_-|$ is large enough we use the following argument. Since $|\phi_-| > |\phi_d|$ we may write

$$\frac{e^{\phi_d}}{-2\sigma_0^*} \ll 1. \quad (79)$$

If ϕ_d is large

$$\cosh \phi_d = Y_d \sim \frac{e^{-\phi_d}}{2} \quad (80)$$

and

$$4\sigma_0^* Y_d \gg 1. \quad (81)$$

If $Y_d \gg 1$ then the symmetric case holds. To obtain an estimate of Y_d to use in Eq. (81) we suggest the following procedure. In the symmetric case, $y_+ - y_d = \sigma^2/2$ and Eq. (37) can be written

$$\int_0^{\sigma^2/2} \frac{dy}{y^{1/2}(y + y_d)} = \sqrt{2}\kappa(d - R_+) \quad (82)$$

neglecting 1 compared to Y_d. This integral is evaluated analytically and gives

$$\tan \frac{y_d^{1/2} \cdot \kappa(d - R_+)}{2} = \frac{\sigma}{(2y_d)^{1/2}}. \quad (83)$$

If we define the following variables

$$p = \frac{y_d^{1/2}\kappa(d - R_+)}{2} \quad (84)$$

$$\sigma' = \frac{\sigma \cdot \kappa(d - R_+)}{2} \quad (85)$$

then Eq. (83) may be rewritten as

$$\tan p = \frac{\sigma'}{p}. \quad (86)$$

Eq. (86) can be used as a tool to determine if the coion is important in swelling pressure calculations. If the calculated value of p for a given set of concentration, ionic radii, plate separation, and surface charge density is large, then the system behaves as a symmetrical case and the coion does not approach the surface. If, however, the value of p is close to 1 and the surface charge is low, then the coion is near the surface and the unsymmetrical case is appropriate.

Only the symmetrical case is important for clays. Using a range of ionic radii from the literature, which are listed in Table 2, we show a dependence of the

Table 2. The sets of ionic radii used to calculate swelling pressures.

Source	Radii (Å)			
	$Li^+(aq)$	$Na^+(aq)$	$K^+(aq)$	$Cs^+(aq)$
Marcus (1983)	2.07	2.37	2.73	3.08
Robinson and Stokes (1959)	3.7	3.3	1.33	1.69
Celeda (1988)	4.51	3.9	3.36	3.07
Coker (1976)	1.94	2.35	2.79	3.16

https://doi.org/10.1346/CCMN.1992.0400502 Published online by Cambridge University Press

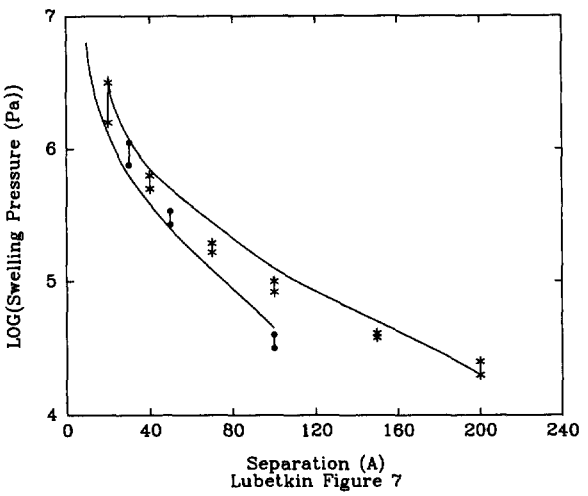

Figure 4. Swelling pressure *vs* separation for Cypern montmorillonite (surface charge density $\sigma_0 = -0.103$ C·m^{-2}) in LiCl(aq) at concentrations of 10^{-2} M and 10^{-4} M. The solid curves are Lubetkin's Figure 7 experimental results (upper 10^{-4} M and lower 10^{-2} M). Theoretical results for a range of Li^+(aq) radii are 10^{-4} M (•—•) and 10^{-2} M (•—•).

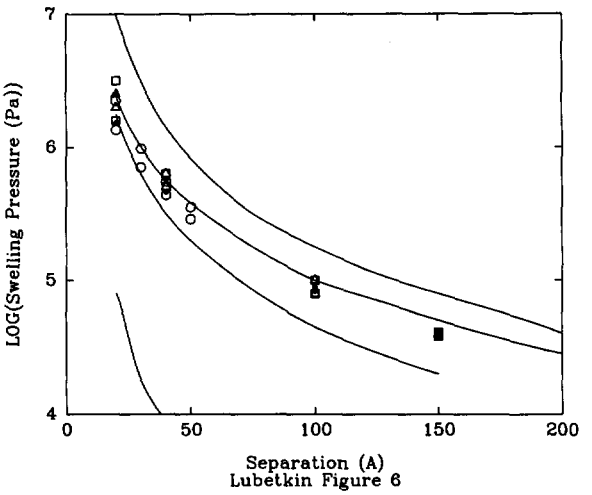

Figure 5. Calculated Log (swelling pressure) *vs* separation for Wyoming bentonite ($\sigma_0 = -0.116$ C·m^{-2}) in 10^{-4} M aqueous solutions of Li^+(aq) (squares), Na^+(aq) (triangles), K^+(aq) (dots) and Cs^+(aq) (circles). Solid lines are Lubetkin's Figure 6 experimental data with the order top to bottom; Li^+(aq), Na^+(aq), K^+(aq), Cs^+(aq).

swelling pressure on the electrolyte counterion present. We compare our results with the experimental results of Lubetkin *et al.* (1984) and Viani *et al.* (1983). In both cases the authors compared their results to the Gouy-Chapman model without accounting for finite size. In a later work Low (1987) compared the Viani results to a constant potential modified Gouy-Chapman model and showed osmotic repulsion is negligible in swelling clays. We will show results obtained with a constant charge modified Gouy-Chapman model compare well with the experimental results.

In Figure 4 we show the swelling pressures for Cypern montmorillonite ($\sigma_0 = -0.103$ C·m^{-2}) in LiCl(aq) at electrolyte concentrations of 10^{-2} M and 10^{-4} M. The solid curves represent the experimental data of Lubetkin *et al.* (1984), with 10^{-4} M for the upper curve and 10^{-2} M for the lower curve. The dots and asterisks represent calculations for 10^{-2} M and 10^{-4} M, respectively, using the range of values of the ionic radius of Li^+(aq) given in Table 2. The two trends are similar, but the agreement in the case of 10^{-2} M is considerably better than for 10^{-4} M.

Huerta and McQuarrie (1991) used the constant surface charge modified Gouy-Chapman model to show the swelling pressure depends on counterion size. Figure 5 shows swelling pressure *vs* separation for Wyoming bentonite in 10^{-4} M aqueous solutions of Li^+(aq), Na^+(aq), K^+(aq), and Cs^+(aq). The solid curves represent the experimental data of Lubetkin *et al.* (1984) with the order from the top being Li^+(aq), Na^+(aq), K^+(aq), and Cs^+(aq). The modified Gouy-Chapman theory not only gives a size-dependence of the cation, but in the correct order. However, the calculated size dependence is not as strong as the data would indicate, particularly for the case of Cs^+(aq).

It is important to point out, however, that montmorillonite can associate in a stacked alignment to form a quasicrystal. A quasicrystal is a structure formed by n unit layers of clay attached one to the other by attractive forces. Between each layer, swelling is not observed. However, swelling is observed between two quasicrystals. It is not clear to what extent quasicrystals form in montmorillonite with monovalent counterions. It is known, however, that the number of unit-layer platelets per particle depends on the exchangeable cation in the order: K^+(aq) > Na^+(aq) > Li^+(aq). Li-montmorillonite does not form quasicrystals; it exists as dispersed unit-layer platelets. Definitive information about quasicrystal formation for Na-montmorillonite is not yet available. If quasicrystal formation occurs in homoionic montmorillonites, the determination of distances of separation between clay platelets in swelling pressure measurements may have been erroneously calculated. Lubetkin *et al.* (1984) report that there were some quasicrystals present in the Na^+(aq) case, more in the K^+(aq) case, and an even greater number in the Cs^+(aq) case. They additionally suggest that this effect may have contributed to lower swelling pressure results, particularly in the case of Cs^+(aq).

In Figure 6 we compare swelling pressure calculations for a series of sodium montmorillonites with different degrees of isomorphic substitutions with experimental data of Viani *et al.* (1983). The electrolyte concentration is 10^{-4} M, and the surface charge density σ_0 for the eight montmorillonites ranges from -0.0924 C·m^{-2} to -0.1868 C·m^{-2}. The greatest value of swell-

https://doi.org/10.1346/CCMN.1992.0400502 Published online by Cambridge University Press

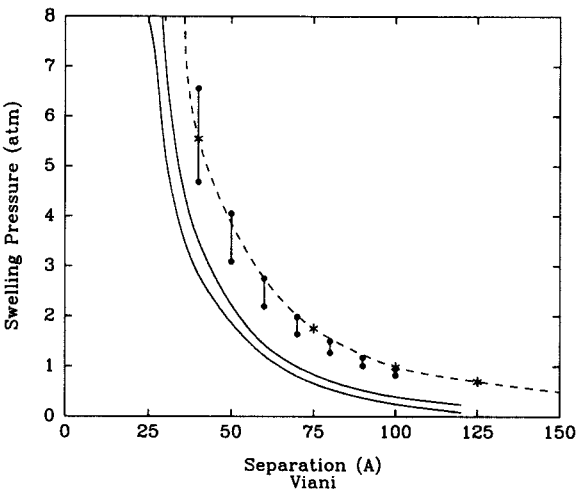

Figure 6. Swelling pressure for montmorillonites with different degrees of isomorphic substitution in 10^{-4} M NaCl(aq). Solid lines mark bounds of Viani *et al.* (1983) experimental data. The range of surface charge densities is -0.0924 C·m^{-2} to -0.1868 C·m^{-2}. The dots mark the range of the theoretical results considering a range of Na^+(aq) radii.

ing pressure corresponds to the montmorillonite with the highest surface charge density. The solid lines give the range of experimental data which was reproduced using the relation between swelling pressures and plate separation given by Eq. (4) of Viani *et al.* (1983). The trend of the calculated values is the same as the trend observed experimentally. We observe that swelling pressure values tend to be independent of the surface charge density for large distances between the two walls.

In Figure 6 we have also plotted the Lubetkin *et al.* (1984) data (dashed line) for sodium Wyoming bentonite ($\sigma_0 = -0.116$ C·m^{-2}) for comparison. Interestingly, Lubetkin's Wyoming bentonite data is above the Viani *et al.* (1983) data which is the opposite of what would be expected if the difference were due to the presence of quasicrystals which do not contribute to the swelling pressure.

We now use the unequal radius model to calculate the swelling pressure in a 1:1 and 2:1 system in which the two counterions are of unequal size. The coion size is not important as shown previously and therefore we consider it to be the same size as the larger counterion for the purpose of calculation. In spite of the importance of such systems, there exists very little experimental swelling pressure data in the literature for mixed electrolyte systems. Therefore we have chosen arbitary ionic radii to compare the unequal size and the same size models. We do not expect our results to be quantitatively comparable with experiments at high divalent ion concentration, due to the well-known failure of the Poisson-Boltzmann equation to accurately reproduce swelling pressure results for divalent electrolytes. However, we will show qualitatively that in a mixed electrolyte both counterion sizes are important in theories of clay swelling pressure.

Table 3. The effect of ionic radii and divalent ion content on swelling pressure (atm).

R_{2+}:R_+	t = 0.50	t = 0.010	t = 0.0001	t = 0.000001
1.5:2.5	1.88	4.76	8.12	8.41
2.5:2.5	2.26	5.30	8.28	8.41
2.5:3.5	2.27	5.44	9.40	9.76

Table 3 contains results of swelling pressure (atm) calculations for three sets of radii (Å) at various values of the parameter t, the divalent electrolyte fraction of the total bulk concentration of 0.0010 M. In the same size case, $R_{2+} = R_+$, the counterion radius is 2.5Å. We contrast the unequal size case by first varying the divalent counterion radius ($R_{2+} = 1.5$Å, $R_+ = 2.5$Å) and secondly by varying the monovalent counterion radius ($R_{2+} = 2.5$Å, $R_+ = 3.5$Å). Clearly the unequal size model predicts results which are significantly different than those of the same size model. At high divalent electrolyte fraction, t = 0.50, a variation of R_{2+} by one angstrom to 1.5Å causes a 17 percent change in the swelling pressure while it is unaffected by a change in R_+ to 3.5Å. At $t = 10^{-6}$ the variation of R_+ has a large effect while a variation in R_{2+} is not important. In the intermediate region in which significant amounts of both electrolyte species are present, a one angstrom variation of either radius causes between a 2 to 13 percent change in swelling pressure.

SUMMARY

The solution to the Poisson-Boltzmann equation for the Unequal Radius Modified Gouy-Chapman model was presented and the swelling pressure calculated. In the case of a 1:1 electrolyte, only the counterion size is important for conditions typical of clay systems. The swelling pressure is calculated for a constant surface charge density and the results are compared with experimental data. Several sets of ionic radii are used to show the swelling pressure depends on the specific counterion in the order Li^+(aq) > Na^+(aq) > K^+(aq) > Cs^+(aq). This is in qualitative agreement with experimental data, however, the degree of dependence of the model result is not nearly as strong. Next we applied the unequal radius model to a 1:1 and 2:1 electrolyte mixture to determine the difference in swelling pressure caused by the unequal size of the two counterions. When the fraction of divalent ion present is small, the monovalent ion size is important. The opposite is true when the fraction of divalent ion is high.

ACKNOWLEDGMENTS

This work has been supported by the National Science Foundation under Grant NSF EAR 8910530.

REFERENCES

Bhuiyan, L. B., Blum, L., and Henderson, D. (1983) The application of the modified Gouy Chapman theory to an electrical double layer containing asymmetric ions: *J. Chem. Phys.* **78(1),** 442–445.

Celeda, J. (1988) On theory of ionic volumes in dilute aqueous solutions of electrolyte: *Collection Czechoslovak Chem. Commun.* **53,** 433–445.

Coker, H. (1976) Polarizability changes on ion hydration: *J. Phys. Chem.* **80(19),** 2084.

Gradshteyn, I. S. and Ryzhik, I. M. (1980) *Table of Integrals, Series and Products:* Academic Press, New York.

Huerta, M. M. and McQuarrie, D. A. (1991) Predicted trend in swelling pressure measurements for lithium, sodium, potassium and cesium montmorillonite: *Electrochimica Acta* **36(11),** 1751–1752.

Low, P. F. (1987) Structural component of the swelling pressure of clays: *Langmuir* **3,** 18–25.

Lubetkin, S. D., Middleton, S. R., and Ottewill, R. H. (1984) Some properties of clay-water dispersions: *Phil. Trans. R. Soc. Lond. A.* **311,** 353–368.

Marcus, Y. (1983) Ionic radii in aqueous solution: *J. Solution Chem.* **12,** 271.

McBroom, R. B. and McQuarrie, D. A. (1987) Interaction of planar double layers in the modified Gouy-Chapman approximation: *Cell Biophys.* **11,** 65–75.

Robinson, R. and Stokes, R. (1959) *Electrolyte Solutions:* Pitman Press, London.

Valleau, J. P. and Torrie, G. M. (1982) The electrical double layer III. Modified Gouy-Chapman theory with unequal ion sizes: *J. Chem. Phys.* **76(9),** 4623–4630.

Viani, B. E., Low, P. F., and Roth, C. B. (1983) Direct measurement of the relation between interlayer force and interlayer distance in the swelling of montmorillonite: *J. Colloid Interface Sci.* **96(1),** 229–244.

(Received 27 February 1992; accepted 21 July 1992; Ms. 2190)